Demonstrating Quantum Speed-Up with a Two-Transmon Quantum Processor.

Andreas Dewes

July 3, 2012

Chapter 1

Introduction & Summary

1.1 Quantum Computing with Superconducting Circuits

This thesis presents experiments performed with a superconducting two-qubit quantum processor. The main goal of this work was to demonstrate a possible quantum computing architecture based on superconducting qubits that follows the canonical blueprint of a quantum processor as sketched in fig. 1.1, in accordance with the five criteria formulated by DiVincenzo [15]. By this definition, a universal quantum computer is a register of well-defined quantum bits (1) with long coherence times (2), on which one can implement any unitary evolution using a universal set of quantum gates (3), fitted with individual high fidelity readout of each qubit (4) and with the possibility to reset the qubits to their ground state (5). Implementing this allegedly simple list of requirements in a system of superconducting qubits has been a major research challenge during the last decade, and is part of more general line of research on superconducting quantum circuits briefly summarized below.

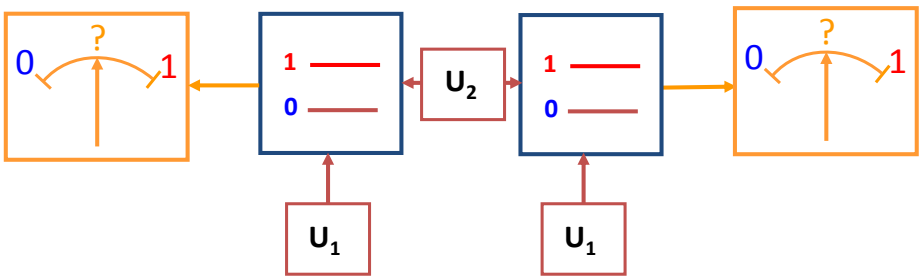

Figure 1.1: The blueprint of a “canonical” two-qubit quantum processor. The two qubits can be individually manipulated (U_1) and a universal two-qubit gate U_2 can be applied to them. Each of the qubits can be read out individually.

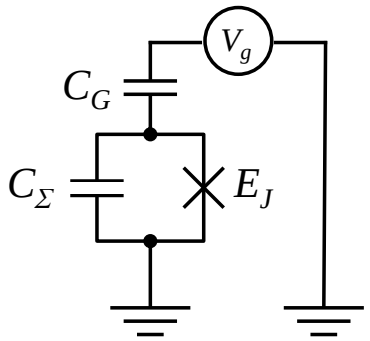

Figure 1.2: The schematic of the simple Cooper pair box (CPB) circuit, consisting of a capacitor in parallel with a Josephson junction capacitively coupled to a voltage source.

1.1.1 Context of this thesis work: 25 years of superconducting quantum circuits

The observation of quantum tunneling in a current-biased Josephson junction switching out of its zero-voltage state by Devoret et. al. [12, 32], first demonstrated that a collective electrical variable such as the superconducting phase difference across a Josephson junction (or the conjugated variable, i.e. the number of Cooper pairs that crossed it) can exhibit quantum properties. Then, the observation of microwave induced transitions between the quantum states of the junction by Martinis et. al. [32] further confirmed the quantum nature of this degree of freedom (See also [32, 33, 6]). A somewhat simpler quantum electrical circuit called the single Cooper Pair Box (CPB), made of a Josephson junction in series with a gate capacitor and a voltage source as shown in fig. 1.2, was later developed in the Quantronics group during the 1990s [4], and its ground state was characterized. With this electrical circuit, Nakamura et. al. [37] performed the first superconducting qubit experiment, demonstrating coherent oscillations between its ground and first excited eigenstates. Although the achieved coherence time was quite short, in the 5-10 ns range, this result attracted a huge interest and triggered the active development of research on superconducting quantum bits.

In the years after, several types of superconducting qubits were proposed using Josephson junctions in different configurations. Different regimes, in which the quantum state of the junctions ranges from almost Cooper pair number states to phase states, were realized. Let us cite here the flux qubit [35, 5] and the phase qubit [34], which were very successful qubits in many aspects. On the side of Cooper Pair Boxes, the Quantronics group made a significant progress by operating a new circuit called the *Quantronium* (Vion *et. al.* [49]), fitted with a strategy for fighting dephasing due to the noise of the electrical control parameters, and with a single-shot readout (although with limited fidelity). The robustness of the quantronium arises from its operation at a so-called *sweet spot* where the qubit frequency is stationary in respect to variations in charge and phase control parameters. The improved coherence of the quantonium allowed to perform all the basic manipulations possible on spins and more generally on

two level systems [8]. Shortly after, another CPB design, inspired from cavity-QED, was developed at Yale by Wallraff et. al. [50]. In this so-called circuit-QED (CQED) design, the CPB, embedded in a microwave resonator, can be thought of as an artificial atom in a resonant cavity. The qubit readout is performed dispersively, i.e. through the cavity pull of the resonator frequency controlled by the qubit state. This small frequency change results in a small phase change of a resonant microwave pulse, which yields –after sufficient repetition– the probability of the two qubit states [3].

Another great bonus of CQED is that the electromagnetic environment in which the qubit relaxes its energy consists of a microwave resonator with a well-controlled impedance. The modern version of the Cooper Pair Box called *Transmon*, follows this design with an extra feature that makes it insensitive to the charge noise which plagues single electron and single Cooper Pair devices. This feature consists in placing the Cooper Pair Box in the phase regime by adding an extra capacitance in parallel with the junction: the qubit frequency is then totally insensitive to the gate charge, and hence to the charge noise to all orders in charge, thus transforming the sweet spot into a "sweet line" in the charge-phase parameter space. This new design, that still leaves sufficient anharmonicity to operate the device as a qubit and allows to drive it, yielded a sizeable improvement in coherence times, qubit robustness and usability. The CQED concept was thus rapidly extended to flux and phase qubits [25].

In 2010, a new type of CQED architecture has been developed by Paik et. al. [39] that combines Transmon qubits with 3D cavities instead of CPW resonators, resulting again in an impressive increase of qubit coherence times of up to two orders of magnitude, with reported qubit relaxation times and coherence times approaching 100 μs. Very recently, these drastically improved coherence times have made possible the realization of elemental quantum feedback and error correction schemes with these systems [48].

The progress achieved during the last decade on the Cooper Pair Box and on the phase qubits has benefited to quantum processors. So far, superconducting CQED processors with up to three qubits have been realized and two- and three-qubit quantum gates [17], multi-qubit entanglement [14, 1] and simple quantum algorithms [13, 31] as well as quantum error correction [42] have recently been demonstrated.

1.1.2 This Thesis Work

At the beginning of this thesis work, CQED processors having demonstrated quantum algorithms did not follow all the rules established by DiVincenzo [15]; in other words, they did not follow the canonical blueprint able to demonstrate quantum speed-up: they were all fitted with a joint readout, which allows to measure the average value of a collective variable of the qubit register, but not each qubit individually. By repeating a given

sequence of gates a large number of times, one can nevertheless determine the quantum state of the qubit register at different steps of the algorithm being run. Since the whole interest of quantum computing is precisely to perform computational tasks more efficiently than with a classical processor, it was essential, in our mind, to demonstrate the quantum speed-up expected from quantum algorithms with a CQED quantum processor fitted with an individual single shot and non-demolishing (QND) readout for each qubit. Such a high fidelity single-shot readout had been developped for a single transmon during a previous thesis in the Quantronics group [30, 40], and it was natural to use it in the present work.

This thesis discusses therefore the realization of a superconducting two-qubit processor based on Transmon qubits, fitted with individual single-shot readouts. In chapter 2, we present the theorical building blocks of this work. Chapter 3 outlines the design of the two-qubit processor, whereas chapter 4 presents the most relevant measurement techniques employed in this work. With the two-qubit processor, we implement elementary one- and two-qubit quantum operations, as detailed in chapter 5. We use it to run a simple quantum algorithm that demonstrates probabilistic quantum speed-up: the Grover search algorithm, as explained in chapter 6. Finally, we discuss in chapter 7 the realization of a four-qubit quantum processor using a more scalable approach that could possibly be extended to an even larger number of qubits.

Note that during this thesis work, quantum speed-up was also demonstrated for the Deutsch-Josza algorithm with a phase qubit processor using individual single-shot and destructive readouts [51].

1.2 Realizing a Two-Qubit Quantum Processor

The quantum processor implemented in this work is shown in Fig. 1.3. It consists of two superconducting quantum bits of the Transmon type, each equipped with its own drive and readout circuit. In order to obtain a high fidelity single-shot readout of the qubit register, we used the Josephson Bifurcation Amplifier (JBA) readout method first developed in the team of Michel Devoret at Yale for the quantronium qubit [45, 47]. This method had indeed already been successfully adapted to the transmon, and yielded a 93 % readout fidelity [30]. In this work, we use a slight variation of this readout type using a nonlinear coplanar-waveguide resonator that serves as a so-called *cavity bifurcation amplifier* (CBA) [44, 47] and which also allows for single-shot readout of the qubit state [30]. Each qubit can be manipulated by driving it with microwave pulses through its readout resonator, allowing robust and fast single-qubit operations. The qubit frequencies can be tuned individually using fast flux lines, allowing us to change the frequency of each qubit over a range of several GHz. The coupling between the two qubits is real-

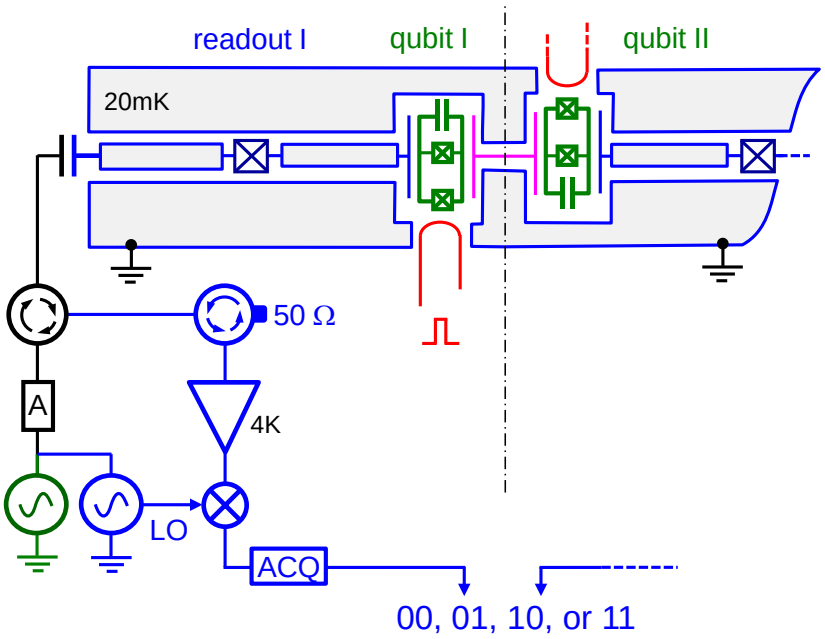

Figure 1.3: Circuit schematic of the two-qubit processor realized in this thesis work, showing the two qubits (in green) coupled by a fixed capacitor (in purple), as well as the fast flux lines (in red) used to tune the qubit frequencies and the qubit readouts (in blue). Each qubit is embedded in its own nonlinear readout resonator and can be driven and read out by microwave reflectometry through an individual microwave line.

ized through a fixed capacitance that connects the two top-electrodes of the Transmons and implements a fixed σ_{xx}-type qubit-qubit coupling. This coupling allows us to generate entangled two-qubit states and to implement a two-qubit gate. We use this simple processor to generate entangled two-qubit states, test the Bell inequality, implement a universal two-qubit gate and perform a simple quantum algorithm that demonstrates quantum speed-up, as will be discussed in the following sections.

1.3 Demonstrating Simultaneous Single-Shot Readout

For readout, each qubit is capacitively coupled to a coplanar waveguide resonator made nonlinear by placing a Josephson junction in its central conductor. We exploit the frequency pull of the bifurcation transition that occurs in such a resonator when driven at a suitable frequency and power to map the qubit states on the bifurcated and non bifurcated cavity states, which are then discriminated by reflectometry. Here, the hysteretic character of the bifurcation transition allows to reduce the measuring power, to latch the cavity state, and to measure it without being affected by subsequent qubit relaxation. The state of the resonator can thus be determined reliably without being limited by qubit relaxation, thereby providing a high-fidelity single-shot qubit readout. Contrary to previ-

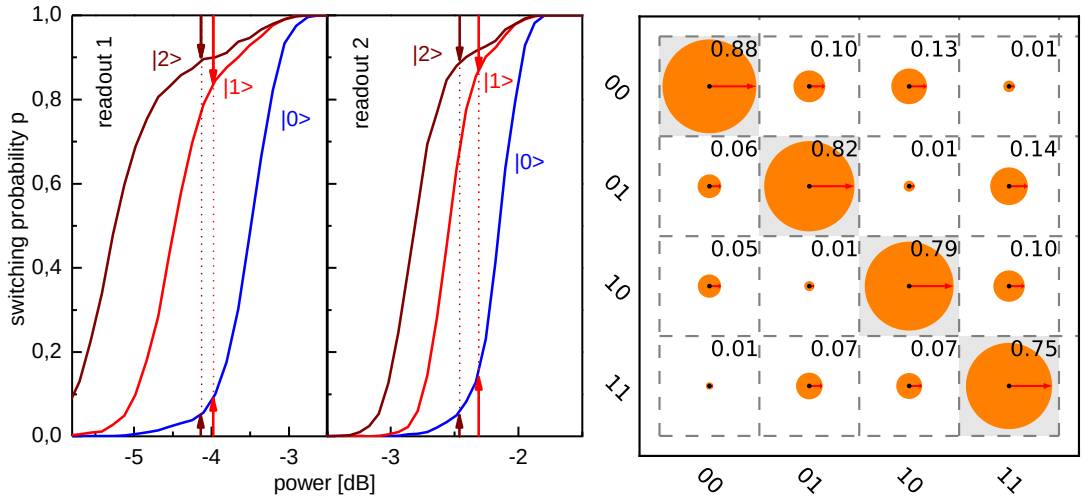

Figure 1.4: a) Switching probabilities of the two readout resonators as a function of the readout drive power at a fixed driving frequency. The measurement is performed after preparing the qubits in the states $|0\rangle$, $|1\rangle$ and $|2\rangle$. The readout contrast is given as the difference in probability between the curves corresponding to the states $|0\rangle$ and $|1\rangle$ or $|2\rangle$, respectively. The highest contrasts of 88 and 89 % are achieved when the qubit is shelved from state $|1\rangle$ to $|2\rangle$. b)Readout matrix of the two-qubit system, giving the probabilities to obtain the different outcomes ij after having prepared the register in the different computational basis states $|kl\rangle$.

ous CQED processors, our processor is fitted with individual readouts, and a simultaneous readout of the full two-qubit register is possible, as requested by the DiVincenzo criteria. For single-qubit CBA readouts, readout fidelities up to 93 % have been achieved [30] by shelving the first excited state of the transmon $|1\rangle$ to the higher excited state $|2\rangle$. However, due to the higher complexity and design constraints of our system, only 83-89 % fidelity has been achieved for the processor presented here. The full characterization of the readout of our processor is shown in fig. 1.4. Figure 1.4a shows the switching probabilities of each individual readout as a function of the drive amplitude, measured at a fixed drive frequency. Individual curves correspond to the qubit being prepared (or shelved) in different states $|0\rangle$, $|1\rangle$ or $|2\rangle$, the difference between either two curves giving the readout contrast between those qubit states. Shelving the qubit from state $|1\rangle$ to state $|2\rangle$ before readout can increase the readout fidelity by more than 10 % and is therefore often used in the experiments presented in this thesis. Figure 1.4b shows the full readout matrix of the two-qubit register that relates measured readout switching probabilities with real qubit state occupation probabilities and allows us to correct readout errors when performing quantum state tomography. In chapter 5 we discuss all relevant readout fidelities and errors in detail and analyze different error sources limiting the readout performance in our experiments.

1.4 Generating and Characterizing Entanglement

The capacitive coupling between the two qubits provides a σ_{xx}-type interaction that can be used to generate entangled two-qubit states. Conveniently, this coupling is only effective when the qubit frequencies are near-resonant and can therefore be effectively switched on and off by tuning the qubit frequencies in and out of resonance. For the processor realized in this work, the effective coupling constant g of the two qubits has been measured as $2g/2\pi = 8.2$ MHz. When the two qubits are in resonance, the effective evolution operator of the two-qubit system is:

$$U(t) = \begin{pmatrix} 1 & 0 & 0 & 0 \\ 0 & \cos 2\pi tg & i\sin 2\pi tg & 0 \\ 0 & i\sin 2\pi tg & \cos 2\pi tg & 0 \\ 0 & 0 & 0 & 1 \end{pmatrix}_{\{|00\rangle,|01\rangle,|10\rangle,|11\rangle\}} \tag{1.1}$$

By using fast flux pulses to non-adiabatically tune the qubits in and out of resonance we can switch on this interaction for a well-defined time. We first characterize the effect of the coupling on the qubit register by preparing the state $|10\rangle$, tuning the qubits in resonance for a given time and measuring the qubit state afterwards. The resulting curve is shown in fig. 1.5a and shows swapping oscillations between the two qubits. Analyzing this curve allows us to extract the effective coupling strength between them. Leaving the interaction between the qubits on for a well-defined time allows us to generate entangled Bell states that we characterize by performing quantum state tomography. The experimental reconstruction of the density matrix of such a Bell-state of the type $|\psi\rangle = (|01\rangle + i\,|10\rangle)/\sqrt{2}$ is shown in fig. 1.5b. The measured fidelity of the prepared state of 91 % and the concurrence of 85 % confirm that entanglement is present in the system. We also characterize the entanglement between the two qubits by measuring the average value of the so-called *Clauser-Horne-Shimony-Holt* operator (CHSH) [7], which combines measurements of the state of the two qubits along different axes on the Bloch sphere and provides a test that can distinguish between classical correlation and quantum entanglement in a two-qubit system.

For classical states, the maximum value of the CHSH operator is bound by 2 but for entangled states it can reach a maximum of $2\sqrt{2}$. Figure 1.6 shows the result of such a CHSH-type measurement performed on a state created by the method described above, showing the value of $\langle\mathrm{CHSH}\rangle$ as a function of the angle ϕ of the measurement basis. We observe a violation of the classical boundary 2 of the operator by 22 standard deviations when correcting the readout errors that are present in our system. The raw, uncorrected data fails to exceed the classical threshold because of readout errors mainly caused by qubit relaxation during the readout. Nevertheless, the observed violation of the equation

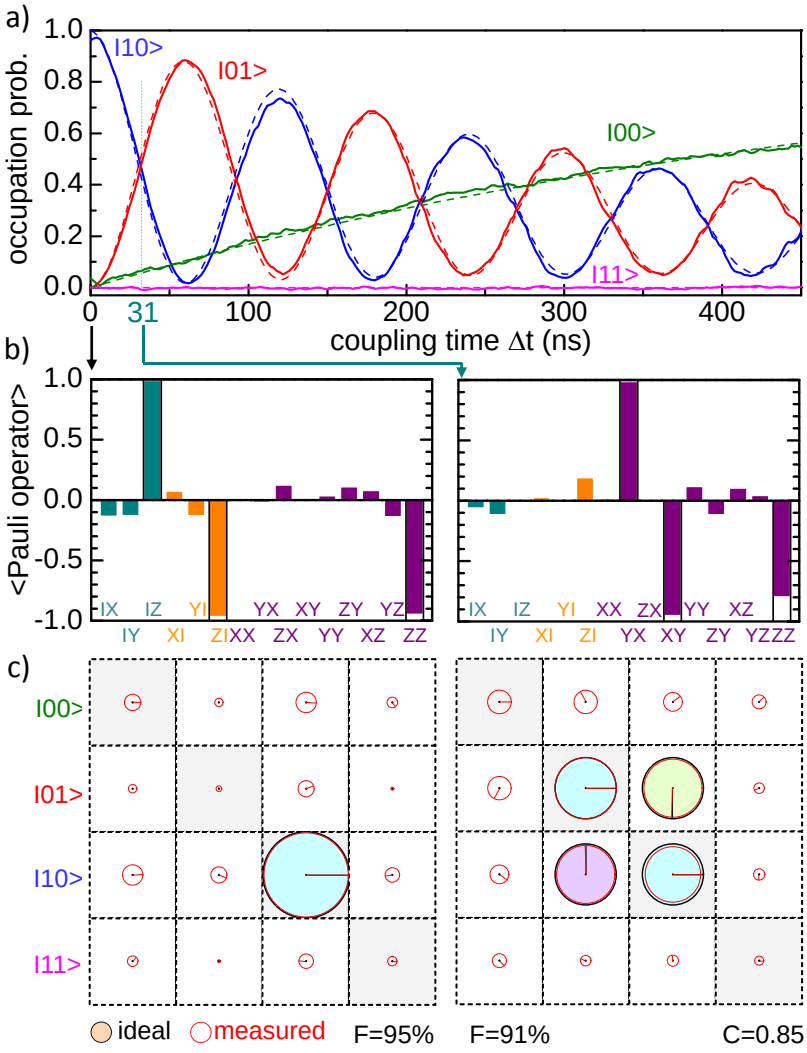

Figure 1.5: Coherent exchange of a single quantum of excitation (swapping oscillations) between the two qubits initially prepared the register state $|10\rangle$, obtained from the resonant interaction between them. a) Register state probabilities as a function of the swapping time Δt. The frequency of the oscillations corresponds to $2g/2\pi = 8.7$ MHz. b) Measured average values of the Pauli operators products $\{I, \sigma_x, \sigma_y, \sigma_z\} \otimes \{I, \sigma_x, \sigma_y, \sigma_z\}$ (Pauli set) for the register states obtained at times 0 ns and 31 ns. c) Corresponding reconstructed density matrices. The area of each circle corresponds to the absolute value of each matrix element and the color and direction of the arrow to the phase of the element. The black circles correspond to the density matrices of the ideal states $|10\rangle$ and $(|10\rangle + i\,|01\rangle)/\sqrt{2}$, respectively.

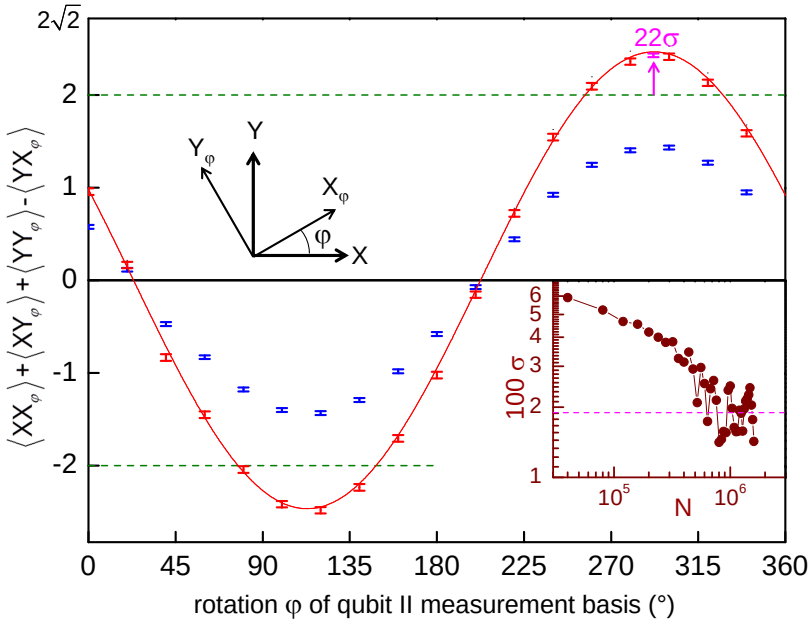

Figure 1.6: Measured average value of CHSH operator for a prepared Bell state. After readout error corrections, the CHSH expectation value (red points) exceeds the classical boundary of 2. The raw measurement data (blue points) lies below this critical threshold. The inset shows the standard deviation σ at the highest point of the curve as a function of the measurement sample size. For the highest sample count, the classical boundary is exceeded by 22 standard deviations.

in the calibrated data is a strong indication of entanglement in the system. A more detailed overview of this experiment can be found in chapter 5.

1.5 Realizing a Universal Two-Qubit Quantum Gate

The swapping evolution given by eq. (1.1) allows not only to prepare entangled two-qubit states but also to implement a universal two-qubit gate: When switching on the interaction for a time $t_{\pi/2} = 1/8g$ one realizes the so-called $\sqrt{i\mathrm{SWAP}}$ gate, represented by the evolution operator

$$U(t) = \begin{pmatrix} 1 & 0 & 0 & 0 \\ 0 & 1/\sqrt{2} & i\sqrt{2} & 0 \\ 0 & i\sqrt{2} & 1/\sqrt{2} & 0 \\ 0 & 0 & 0 & 1 \end{pmatrix}_{\{|00\rangle,|01\rangle,|10\rangle,|11\rangle\}} \tag{1.2}$$

which forms together with single qubit gates a universal set of gates, on which any algorithm can be decomposed. We characterize the operation and errors of our implementation of this gate by performing quantum process tomography, obtaining a gate fidelity of 90 % . The 10 % error in gate fidelity is caused mainly by qubit relaxation and

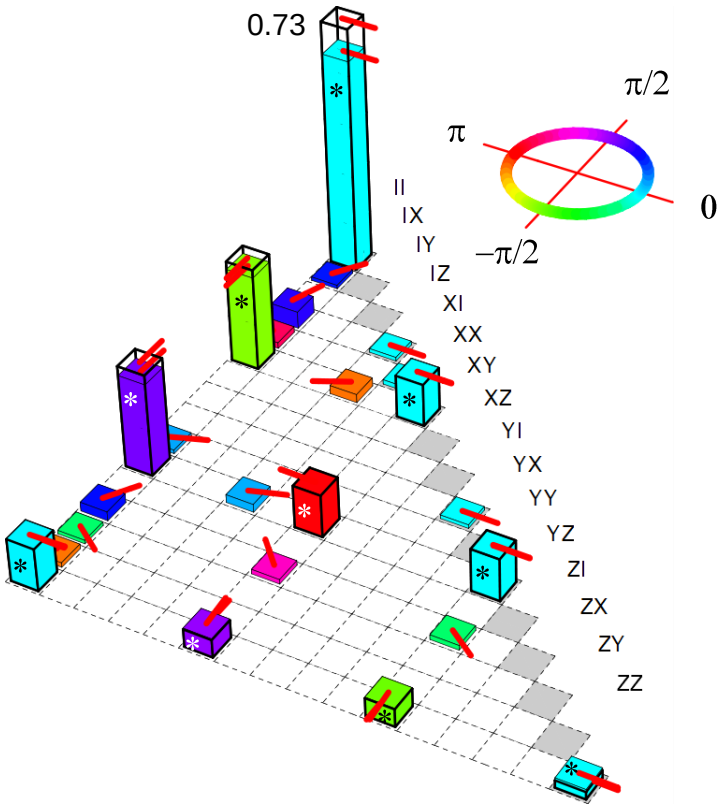

Figure 1.7: Measured χ-matrix of the implemented $\sqrt{i\mathrm{SWAP}}$ gate. The row labels correspond to the indices of the E_i Pauli operators, the height of each bar to the absolute value of the corresponding matrix element, and the color and red arrow direction to the argument of the element. The ideal χ-matrix of the $i\sqrt{\mathrm{SWAP}}$ gate is given by the outlined bars. The upper half of the positive-hermitian matrix is not shown.

dephasing during the gate operation and only marginally by deterministic preparation errors, as will be discussed in chapter 5. Figure 1.7 shows the measured χ matrix of the gate, that describes its effect in the Pauli basis of two-qubit operators. The χ matrix provides the full information on the unitary and non-unitary action of the gate. The achieved fidelity of the gate operation is sufficient to allow the implementation of simple quantum algorithms with our processor.

1.6 Running a Quantum Search Algorithm

Using a two-qubit quantum gate related to the one described above, we run a simple quantum algorithm on our processor, the so called *Grover search algorithm* [22]. The version of this algorithm that we implement operates on the two-qubit basis $x_i \in \{ |00\rangle , |01\rangle, |10\rangle , |11\rangle\}$ and can distinguish between four different *Oracle functions* $\mathcal{C}_j(x)$ with $x \in x_i$ that give $\mathcal{C}_j(x = x_j) = 1$ and $\mathcal{C}_j(x \neq x_j) = 0$. In the two-qubit case, this algorithm requires only one evaluation of the Oracle function $\mathcal{C}_j(x)$, implemented as a unitary operator, to determine which state among the four possible ones it tags. This case thus provides a simple benchmark of the operation of the quantum processor, and a simple and illustrative example of quantum speed-up in comparison with classical algorithms, as discussed in chapter 6. The diagram of the Grover search algorithm implemented

in our processor is shown in fig. 1.8a and involves two $i\mathrm{SWAP}$ gate operations and six single-qubit operations along with a single-shot qubit readout at the end of the algorithm. We measure the success probability of the algorithm from the obtained outcomes, and complete the analysis of its operation by performing the tomography of the quantum state at different steps of the algorithm. We first discuss this evolution that sheds light on how quantum speed-up is achieved.

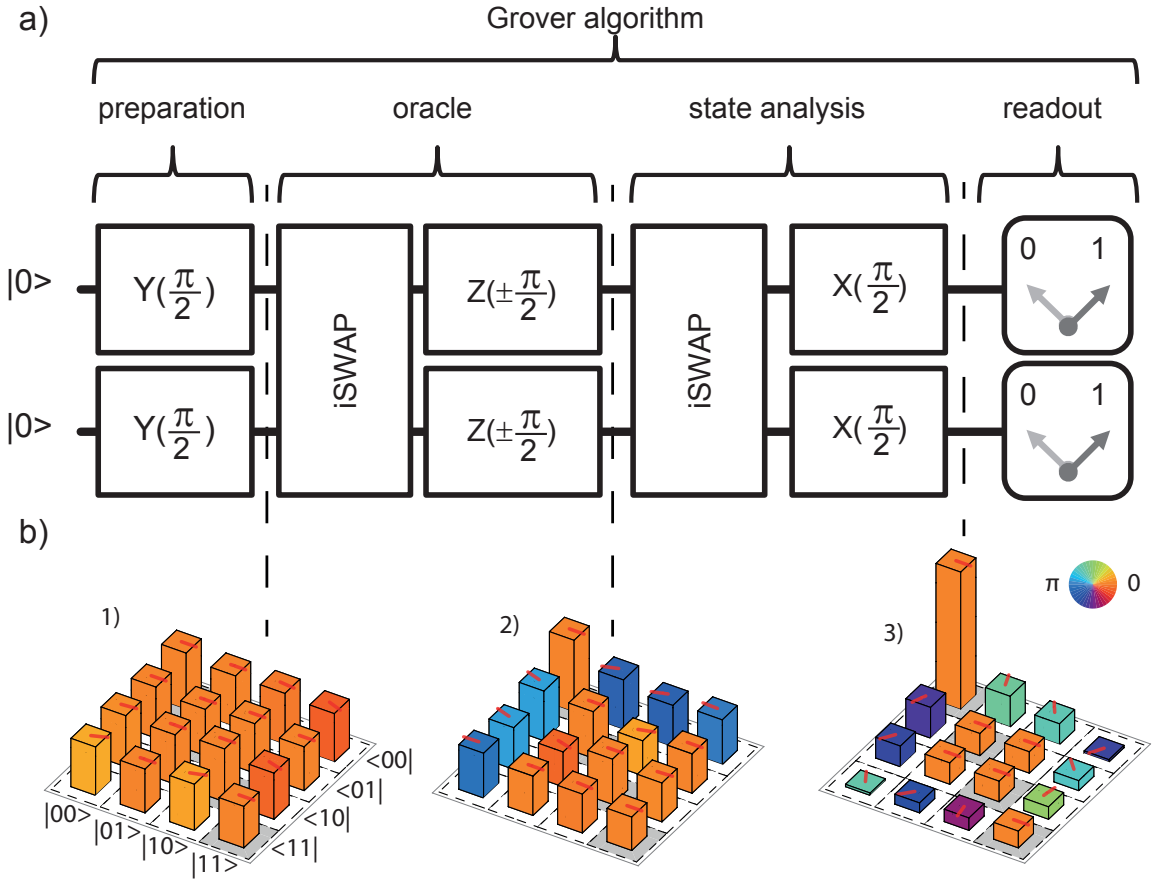

Figure 1.8: a) A two-qubit version of the Grover search algorithm that we implemented on our quantum processor. The algorithm consists in preparing a fully superposed state, applying a given Oracle operator to it only once, and analyzing the resulting output to determine the quantum state tagged by this Oracle operator. b) Measured density matrices when running the Grover search algorithm with a search oracle marking the state $|00\rangle$. 1) shows the state after the generalized Hadamard transform, 2) after applying the quantum oracle and 3) after the final step of the algorithm.

Fig. 1.8b shows the density matrices determined experimentally when running the Grover search algorithm with the Oracle operator tagging the state $|00\rangle$. State tomography is first shown after preparation with a generalized Hadamard transform applied to the initial state $|00\rangle$. It clearly corresponds to a superposition of all the computational basis states. The quantum state after having applied the quantum Oracle is $-|00\rangle + |01\rangle + |10\rangle + |11\rangle$ and the information on the tagged state is encoded in the

phase of the state $|00\rangle$. After extracting this phase information, the tomography displays a large peak on state $|00\rangle$ at the end of the algorithm, just as expected. The fidelity of the final quantum state of the algorithm is 68%, 61%, 64% and 65% for the four different Oracle operators, respectively. These fidelities, corrected for readout errors, do not quantify the quantum speed-up achieved when running the algorithm. For this, it is necessary to analyze the results obtained after a single run, which does not allow for any corrections of the readout outcomes.

1.7 Demonstrating Quantum Speed-Up

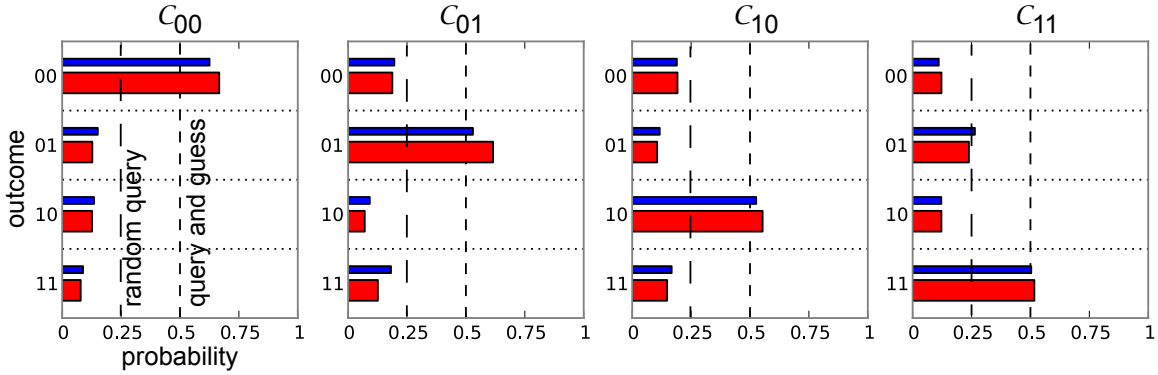

Figure 1.9: Single-run results when running the Grover search algorithm on our two-qubit quantum processor. Shown are the probabilities of measuring the qubit register in state $|i\rangle$ for an Oracle function $\mathcal{C}_j$ marking the state $|j\rangle$ provided to the algorithm. In all four cases, the success probability of the algorithm is $> 50\%$, thus outperforming any classical "random query" or "query and guess" algorithm using a single Oracle call.

The main interest of running a quantum algorithm is to obtain an advantage in the run-time in comparision to a classical algorithm, the so-called *quantum speed-up*. To characterize this speed-up as obtained with our processor, we run the Grover algorithm for all four possible Oracle functions and directly read out the state of the qubit register after the last step of the algorithm instead of performing quantum state tomography, thus not correcting any readout errors. By averaging the outcomes of many such individual runs of the algorithm with different Oracle functions we obtain the so-called *single-run fidelities*, which –for the four different Oracle functions– have been measured as 66%, 55%, 61% and 52%. The full probability distributions for the four possible cases are shown in fig. 1.9. The achieved success probability is always lower than the theoretically possible value of 100 %, mainly because of relaxation and decoherence of the qubit state during the runtime of the algorithm and –to a small degree– errors in the pulse sequence. The measured success probabilities are however larger than the 50% success probability of a classical query-and-guess algorithm using the outcome of a sin-

gle query. The algorithm thus demonstrates quantum speed-up, as explained in greater detail in chapter 6.

1.8 Towards a Scalable Multi-Qubit Architecture

The approach to superconducting quantum computing outlined in the previous sections is well suited for the implementation of simple quantum processors with a few qubits. Hovewer, due to several design limitations it is not suitable for implementing a large scale quantum computer. As an example, the direct qubit-qubit coupling employed in this thesis work is not suitable for coupling a large number of qubits since it becomes increasingly difficult to deterministically switch on and off the coupling between individual qubits as the number of qubits increases, a problem sometimes referred to as “frequency crowding”. Also, fitting each qubit of the processor with individual drive and readout circuitry –as done in this work– is usually not extensible to a large number of qubits due to topological and space constraints on the chip, as well as financial and practical constraints for a cryogenic experimental setup.

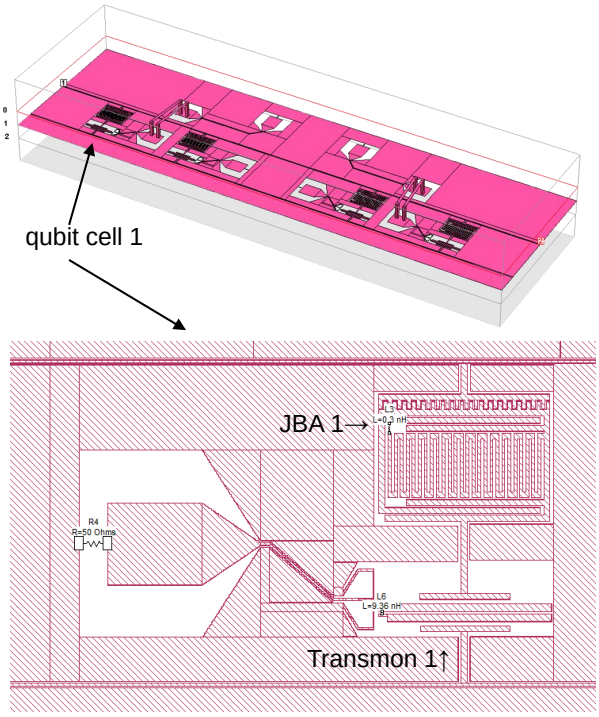

Figure 1.10: Schematic of the four-qubit chip realized in this thesis work. Shown on top is the whole chip with connectors for the drive and readout transmission line and for the four fast flux lines. Below we show a single qubit cell with a Transmon qubit coupled to the quantum bus, a fluxline and a JBA readout.

Recently, several research groups have started to address these issues by devising new architectures for superconducting quantum processors that can –in theory– be scaled to a very large number of qubits. Here we will mention only the so-called “Rez-Qu” architecture [19] and the surface-code approach [16] pursued e.g. by IBM. In this thesis work we discuss our own approach towards scalable quantum computing, where we have developed a revised version of our qubit chip that provides a way to implement a system with a larger –albeit still small– number of qubits. Key elements of this architecture are a quantum bus in form of a high-Q microwave resonator that is used for coupling the qubits and a multiplexed drive and readout circuit that allows us to measure

and manipulate all qubits through one single microwave transmission line.

Figure 1.10 shows the schematic of the first version of this architecture. Our chip contains four Transmon qubits which are capacitively coupled to a distributed high-Q resonator acting as a quantum bus. In addition, each qubit is coupled to a low-Q non-linear lumped element resonator acting as a JBA, which is used for reading out the qubit state. Each of these resonators is in turn coupled capacitively to the input transmission line. The resonance frequencies of the readout resonators are arranged in ascending order with a frequency spacing of ≈ 50 MHz between adjacent resonators. This frequency spacing allows us to address each resonator individually and to read out the state of the full qubit register in parallel using only one single transmission line. Fig. 1.11 shows the measured $|S_{12}|$ matrix element of such a chip with four JBA resonators at frequencies between 6.78 GHz and 6.95 GHz, plotted as a function of the incident microwave power. The "knee" in each of the four resonance curves appearing between -45 and -40 dBm corresponds to the bifurcation point of the resonators.

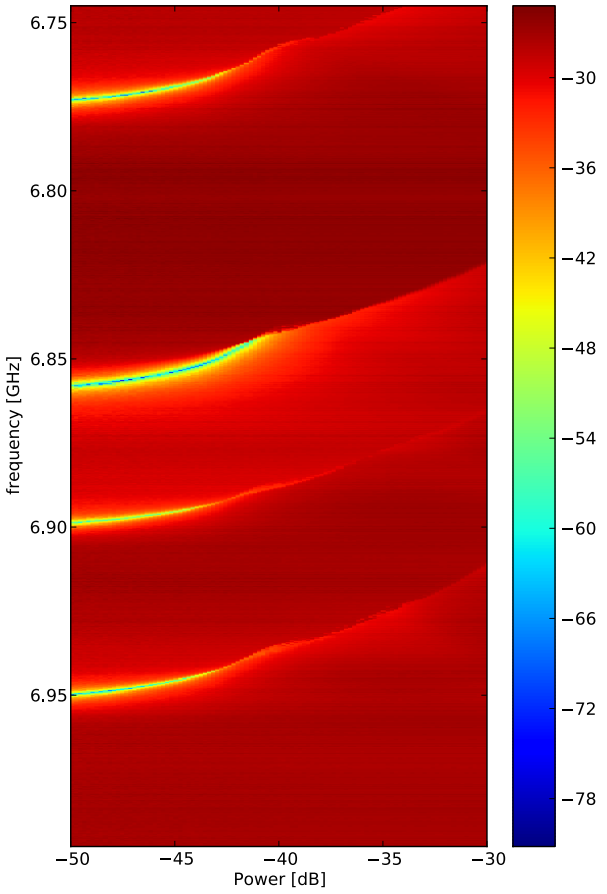

Figure 1.11: The measured $|S_{12}|$ tranmission coefficient for the input transmission line of our four-qubit chip. Clearly visible are four resonances of the JBA resonators and the bifurcation of each resonator at high input power.

Still, this approach suffers from a relatively bad ON/OFF ratio in the qubit-qubit coupling. To alleviate this problem, the Transmon qubit used in the current version of this architecture can be replaced by a qubit with a tunable coupling [46]. Alternatively, it is possible to use a fixed-frequency coupling scheme for the qubits, thereby altogether eliminating the need for frequency tuning of individual qubits and also reducing the number of input transmission lines from $n + 1$ to 1, where n is the number of qubits.

A detailed discussion of the scalable architecture and the first preliminary measurements performed with a four-qubit chip are presented in chapter 7 of this thesis.

Bibliography

[1] M. Ansmann, H. Wang, R. C. Bialczak, M. Hofheinz, E. Lucero, M. Neeley, A. D. O'Connell, D. Sank, M. Weides, J. Wenner, A. N. Cleland, and J. M. Martinis. Violation of bell's inequality in josephson phase qubits. *Nature*, 461(7263):504–506, 2009.

[2] A. Blais, J. Gambetta, A. Wallraff, D. I. Schuster, S. M. Girvin, M. H. Devoret, and R. J. Schoelkopf. Quantum-information processing with circuit quantum electrodynamics. *Physical Review A*, 75(3):032329, Mar. 2007.

[3] A. Blais, R. Huang, A. Wallraff, S. M. Girvin, and R. J. Schoelkopf. Cavity quantum electrodynamics for superconducting electrical circuits: An architecture for quantum computation. *Physical Review A*, 69(6):062320, June 2004.

[4] V. Bouchiat, D. Vion, P. Joyez, D. Esteve, and M. H. Devoret. Quantum coherence with a single cooper pair. *Physica Scripta*, T76(1):165, 1998.

[5] I. Chiorescu, Y. Nakamura, C. J. P. M. Harmans, and J. E. Mooij. Coherent quantum dynamics of a superconducting flux qubit. *Science*, 299(5614):1869 –1871, Mar. 2003.

[6] J. Clarke, A. N. Cleland, M. H. Devoret, D. Esteve, and J. M. Martinis. Quantum mechanics of a macroscopic variable: The phase difference of a josephson junction. *Science*, 239(4843):992–997, Feb. 1988.

[7] J. F. Clauser, M. A. Horne, A. Shimony, and R. A. Holt. Proposed experiment to test local Hidden-Variable theories. *Physical Review Letters*, 23(15):880–884, Oct. 1969.

[8] E. Collin, G. Ithier, A. Aassime, P. Joyez, D. Vion, and D. Esteve. NMR-like control of a quantum bit superconducting circuit. *Physical Review Letters*, 93(15):157005, Oct. 2004.

[9] A. Cottet. *Implementation of a quantum bit in a superconducting circuit*. PhD thesis, Université Paris VI, Paris, 2002.

[10] D. Deutsch. Quantum theory, the Church-Turing principle and the universal quantum computer. *Proceedings of the Royal Society of London. A. Mathematical and Physical Sciences*, 400(1818):97 –117, July 1985.

[11] M. Devoret. Quantum fluctuations in electrical circuits. In *Les Houches Session on Quantum Fluctuations*, volume LXIII, pages 351–386. 1995.

[12] M. H. Devoret, J. M. Martinis, and J. Clarke. Measurements of macroscopic quantum tunneling out of the Zero-Voltage state of a Current-Biased josephson junction. *Physical Review Letters*, 55(18):1908–1911, Oct. 1985.

[13] L. DiCarlo, J. M. Chow, J. M. Gambetta, L. S. Bishop, B. R. Johnson, D. I. Schuster, J. Majer, A. Blais, L. Frunzio, S. M. Girvin, and R. J. Schoelkopf. Demonstration of two-qubit algorithms with a superconducting quantum processor. *Nature*, 460(7252):240–244, July 2009.

[14] L. DiCarlo, M. D. Reed, L. Sun, B. R. Johnson, J. M. Chow, J. M. Gambetta, L. Frunzio, S. M. Girvin, M. H. Devoret, and R. J. Schoelkopf. Preparation and measurement of three-qubit entanglement in a superconducting circuit. *Nature*, 467(7315):574–578, 2010.

[15] D. P. DiVincenzo. The physical implementation of quantum computation. *Fortschritte der Physik*, 48(9-11):771–783, Sept. 2000.

[16] D. P. DiVincenzo. Fault-tolerant architectures for superconducting qubits. *Physica Scripta*, T137:014020, Dec. 2009.

[17] A. Fedorov, L. Steffen, M. Baur, and A. Wallraff. Implementation of a toffoli gate with superconducting circuits. *arXiv:1108.3966*, Aug. 2011.

[18] R. Feynman. Simulating physics with computers. *International Journal of Theoretical Physics*, 21(6):467–488, 1982.

[19] A. Galiautdinov, A. N. Korotkov, and J. M. Martinis. Resonator–zero-qubit architecture for superconducting qubits. *Physical Review A*, 85(4):042321, Apr. 2012.

[20] M. Göppl, A. Fragner, M. Baur, R. Bianchetti, S. Filipp, J. M. Fink, P. J. Leek, G. Puebla, L. Steffen, and A. Wallraff. Coplanar waveguide resonators for circuit quantum electrodynamics. *Journal of Applied Physics*, 104(11):113904–113904–8, Dec. 2008.

[21] L. K. Grover. A fast quantum mechanical algorithm for database search. In *Proceedings of the twenty-eighth annual ACM symposium on Theory of computing*, STOC '96, page 212–219, New York, NY, USA, 1996. ACM.

[22] L. K. Grover. Quantum mechanics helps in searching for a needle in a haystack. *Physical Review Letters*, 79(2):325–328, July 1997.

[23] L. K. Grover. From schrödinger's equation to the quantum search algorithm. *American Journal of Physics*, 69(7):769–777, 2001.

[24] S. Haroche and J. Raimond. *Exploring the Quantum: Atoms, Cavities and Photons*. Oxford University Press, 2006.

[25] M. Hofheinz, H. Wang, M. Ansmann, R. C. Bialczak, E. Lucero, M. Neeley, A. D. O'Connell, D. Sank, J. Wenner, J. M. Martinis, and A. N. Cleland. Synthesizing arbitrary quantum states in a superconducting resonator. *Nature*, 459(7246):546–549, May 2009.

[26] B. Josephson. Possible new effects in superconductive tunnelling. *Physics Letters*, 1(7):251–253, July 1962.

[27] J. Koch, T. M. Yu, J. Gambetta, A. A. Houck, D. I. Schuster, J. Majer, A. Blais, M. H. Devoret, S. M. Girvin, and R. J. Schoelkopf. Charge-insensitive qubit design derived from the cooper pair box. *Physical Review A*, 76(4):042319, Oct. 2007.

[28] B. P. Lanyon, C. Hempel, D. Nigg, M. Müller, R. Gerritsma, F. Zähringer, P. Schindler, J. T. Barreiro, M. Rambach, G. Kirchmair, M. Hennrich, P. Zoller, R. Blatt, and C. F. Roos. Universal digital quantum simulation with trapped ions. *Science*, 334(6052):57–61, July 2011.

[29] S. Lloyd. Universal quantum simulators. *Science*, 273(5278):1073–1078, Aug. 1996.

[30] F. Mallet, F. R. Ong, A. Palacios-Laloy, F. Nguyen, P. Bertet, D. Vion, and D. Esteve. Single-shot qubit readout in circuit quantum electrodynamics. *Nat Phys*, 5(11):791–795, Nov. 2009.

[31] M. Mariantoni, H. Wang, T. Yamamoto, M. Neeley, R. C. Bialczak, Y. Chen, M. Lenander, E. Lucero, A. D. O'Connell, D. Sank, M. Weides, J. Wenner, Y. Yin, J. Zhao, A. N. Korotkov, A. N. Cleland, and J. M. Martinis. Implementing the quantum von neumann architecture with superconducting circuits. *Science*, 334(6052):61 –65, Oct. 2011.

[32] J. M. Martinis, M. H. Devoret, and J. Clarke. Energy-Level quantization in the Zero-Voltage state of a Current-Biased josephson junction. *Physical Review Letters*, 55(15):1543–1546, Oct. 1985.

[33] J. M. Martinis, M. H. Devoret, and J. Clarke. Experimental tests for the quantum behavior of a macroscopic degree of freedom: The phase difference across a josephson junction. *Physical Review B*, 35(10):4682–4698, Apr. 1987.

[34] J. M. Martinis, S. Nam, J. Aumentado, and C. Urbina. Rabi oscillations in a large Josephson-Junction qubit. *Physical Review Letters*, 89(11):117901, 2002.

[35] J. E. Mooij, T. P. Orlando, L. Levitov, L. Tian, C. H. van der Wal, and S. Lloyd. Josephson Persistent-Current qubit. *Science*, 285(5430):1036 –1039, 1999.

[36] F. Motzoi, J. M. Gambetta, P. Rebentrost, and F. K. Wilhelm. Simple pulses for elimination of leakage in weakly nonlinear qubits. *Physical Review Letters*, 103(11):110501, 2009.

[37] Y. Nakamura, Y. A. Pashkin, and J. S. Tsai. Coherent control of macroscopic quantum states in a single-Cooper-pair box. *Nature*, 398(6730):786–788, Apr. 1999.

[38] M. A. Nielsen and I. L. Chuang. *Quantum Compuation and Quantum Information*. Cambridge University Press, 2000.

[39] H. Paik, D. I. Schuster, L. S. Bishop, G. Kirchmair, G. Catelani, A. P. Sears, B. R. Johnson, M. J. Reagor, L. Frunzio, L. I. Glazman, S. M. Girvin, M. H. Devoret, and R. J. Schoelkopf. Observation of high coherence in josephson junction qubits measured in a Three-Dimensional circuit QED architecture. *Physical Review Letters*, 107(24):240501, Dec. 2011.

[40] A. Palacios-Laloy. *Superconducting Qubit in a Resonator: Test of the Leggett-Garg Inequality and Single-Shot Readout*. PhD thesis, Commissariat à l'Energie Atomique, Saclay, 2010.

[41] D. M. Pozar. *Microwave Engineering*. Wiley, 4 edition, Nov. 2011.

[42] M. D. Reed, L. DiCarlo, S. E. Nigg, L. Sun, L. Frunzio, S. M. Girvin, and R. J. Schoelkopf. Realization of Three-Qubit quantum error correction with superconducting circuits. *arXiv:1109.4948*, Sept. 2011.

[43] D. I. Schuster. *Circuit Quantum Electrodynamics*. PhD thesis, Yale University, New Haven, 2007.

[44] I. Siddiqi, R. Vijay, M. Metcalfe, E. Boaknin, L. Frunzio, R. J. Schoelkopf, and M. H. Devoret. Dispersive measurements of superconducting qubit coherence with a fast latching readout. *Physical Review B*, 73(5):054510, Feb. 2006.

[45] I. Siddiqi, R. Vijay, F. Pierre, C. M. Wilson, M. Metcalfe, C. Rigetti, L. Frunzio, and M. H. Devoret. RF-Driven josephson bifurcation amplifier for quantum measurement. *Physical Review Letters*, 93(20):207002, Nov. 2004.

[46] S. J. Srinivasan, A. J. Hoffman, J. M. Gambetta, and A. A. Houck. Tunable coupling in circuit quantum electrodynamics using a superconducting charge qubit with a V-Shaped energy level diagram. *Physical Review Letters*, 106(8):083601, Feb. 2011.

[47] R. Vijay, M. H. Devoret, and I. Siddiqi. Invited review article: The josephson bifurcation amplifier. *Review of Scientific Instruments*, 80(11):111101–111101–17, Nov. 2009.

[48] R. Vijay, C. Macklin, D. H. Slichter, S. J. Weber, K. W. Murch, R. Naik, A. N. Korotkov, and I. Siddiqi. Quantum feedback control of a superconducting qubit: Persistent rabi oscillations. *arXiv:1205.5591*, May 2012.

[49] D. Vion, A. Aassime, A. Cottet, P. Joyez, H. Pothier, C. Urbina, D. Esteve, and M. H. Devoret. Manipulating the quantum state of an electrical circuit. *Science*, 296(5569):886 –889, May 2002.

[50] A. Wallraff, D. I. Schuster, A. Blais, L. Frunzio, R.-S. Huang, J. Majer, S. Kumar, S. M. Girvin, and R. J. Schoelkopf. Strong coupling of a single photon to a superconducting qubit using circuit quantum electrodynamics. *Nature*, 431(7005):162–167, 2004.

[51] T. Yamamoto, M. Neeley, E. Lucero, R. C. Bialczak, J. Kelly, M. Lenander, M. Mariantoni, A. D. O'Connell, D. Sank, H. Wang, M. Weides, J. Wenner, Y. Yin, A. N. Cleland, and J. M. Martinis. Quantum process tomography of two-qubit controlled-Z and controlled-NOT gates using superconducting phase qubits. *Physical Review B*, 82(18):184515, Nov. 2010.

[52] B. Yurke and J. S. Denker. Quantum network theory. *Physical Review A*, 29(3):1419–1437, Mar. 1984.